Journal of Catalysis **205,** 135–146 (2002)
doi:10.1006/jcat.2001.3433, available online at http://www.idealibrary.com on IDEAL®

Understanding the Influence of the Pretreatment Procedure on Platinum Particle Size and Particle-Size Distribution for SiO_2 Impregnated with $[Pt^{2+}(NH_3)_4](NO_3^-)_2$: A Combination of HRTEM, Mass Spectrometry, and Quick EXAFS

M. K. Oudenhuijzen,* P. J. Kooyman,† B. Tappel,* J. A. van Bokhoven,* and D. C. Koningsberger*,[1]

*Department of Inorganic Chemistry and Catalysis, Debye Institute, Utrecht University, Utrecht, The Netherlands; and †National Centre for High Resolution Electron Microscopy, Delft University of Technology, Delft, The Netherlands

Received June 5, 2001; revised September 24, 2001; accepted September 28, 2001

Using a combination of mass spectrometry, *in situ* quick extended X-ray absorption fine structure, high-resolution transmission electron microscopy, and hydrogen chemisorption, we studied the reactions taking place during different pretreatments of the catalyst precursor $[Pt^{2+}(NH_3)_4](NO_3^-)_2$ impregnated on high-surface-area SiO_2 (400 m^3/g). Direct reduction in hydrogen leads to the formation of Pt metal particles in the temperature range of 150–200°C in a fast process. The reduction is accompanied by sintering of the platinum particles, leading to relatively large particles, with an average particle size of approximately 14–16 Å. Autoreduction in helium leads to multiple steps in the reduction. Around 210 and 240°C, NO_x released due to the decomposition of NH_4NO_3, formed during heating up to 180–200°C, reduces the catalyst precursor at a high rate. At higher temperatures, the reduction continues slowly through an autoreduction of the $Pt(NH_3)_x^{2+}$ complex. The slow reduction rate suggests a nonmobile species. Accordingly, the final metal-particle size is small, with particles of 10–12 Å. Calcination–reduction results in large particles via a similar decomposition of NH_4NO_3. Particle-size distribution after autoreduction is considerably smaller than after direct reduction. The key to obtaining small particles with a relatively narrow-sized distribution is to avoid the formation of mobile species. With impregnated $[Pt^{2+}(NH_3)_4](NO_3^-)_2$, this is best achieved by autoreduction.

Key Words: **Pt; $Pt(NH_3)_4(NO_3)_2$; SiO_2; QEXAFS; pretreatment; impregnation; dispersion; mass spectrometry.**

INTRODUCTION

A straightforward method for loading a metal precursor of a supported heterogeneous transition-metal catalyst is incipient wetness impregnation (1, 2). Typically, a metal precursor is dissolved in an aqueous solution and brought into the pores of the support. To remove all ligands and obtain metal particles, the impregnated support has to be pretreated. Generally, pretreatment consists of several temperature-programmed steps in different gaseous environments (for example, H_2, He, or O_2). This pretreatment process is crucial for the final metal-particle size and particle-size distribution (3). Since catalysis is a surface process, small particle sizes are crucial in order to have a high fraction of catalytic-active surface atoms. Also, small particles are in general more active in catalysis. In addition, it has been reported repeatedly that the support largely influences the catalytic properties of supported catalysts (4–7). If this metal-support interaction is well understood, this promises the possibility of tailor-made catalysts. In order to understand these metal-support effects it is crucial to be able to prepare different particle sizes on a support with a narrow particle-size distribution. This can only be done when the pretreatment processes leading to certain metal-particle sizes and distributions are well understood.

The metal precursor can be one of a variety of complexes. Commonly used precursors for Pt are H_2PtCl_6 (8–13), $Pt(NH_3)_4(NO_3)_2$ (14), and $Pt(acac)_2$ (12, 15, 16). Each precursor has its own unique properties. The choice of precursor therefore depends on such parameters as support properties and the requirements for the final metal-particle size. A disadvantage of H_2PtCl_6 is that the presence of chlorine alters the acidity of the support material (17) and can poison the catalyst. Platinum acetylacetonate $[Pt(acac)_2]$ is reported to result in highly dispersed particles (12). A disadvantage of this precursor is the use of organic solvents, which can result in carbonaceous residues on the catalyst and organic waste. $Pt(NH_3)_4(NO_3)_2$ overcomes these disadvantages. It can be used in aqueous solutions and all ligands can be removed by heating the sample. For these reasons, $Pt(NH_3)_4(NO_3)_2$ on a SiO_2 precursor was used in this study.

Typical studies of the pretreatment of $Pt(NH_3)_4(NO_3)_2$ deal with a trial-and-error variation of the pretreatment, resulting in different metal-particle sizes (e.g., 3). For pretreatments involving zeolitic supports, generally it is

[1] To whom correspondence should be addressed. Fax: +31 30 251 1027. E-mail: d.c.koningsberger@chem.uu.nl.

0021-9517/02 $35.00

found that slow heating rates (e.g., 0.2°C/min) are crucial for small particle sizes (18, 19). This is caused by the microporous structure of zeolites, which adsorb water strongly. H_2O present during pretreatment steps generally results in large particles (18). For macroporous supports such as SiO_2, this is much less of a problem. Water desorbs easily at relatively low temperatures. Therefore, heating rates during pretreatments involving macroporous supports can be high compared to zeolites (e.g., 3).

Several studies that give some insight into the chemical processes taking place during the pretreatment processes have been performed (18, 20). Kinoshita *et al.* (20) studied the thermal stability of several metal precursors, including $[Pt^{2+}(NH_3)_4](NO_3^-)_2$, in air and hydrogen. It was found for all precursors that thermal stability in air is higher than in hydrogen.

Dalla Betta and Boudart (21) studied the pretreatment of $Pt(NH_3)_4^{2+}$ exchanged on zeolite Y. They report that direct reduction in H_2 leads to the formation of neutral $Pt(NH_3)_2H_2$ hydride in the temperature range of 80–100°C, ultimately resulting in agglomeration and thus large particles. They conclude that decomposition of the complex in O_2 should be carried out prior to the reduction.

Van den Broek *et al*. (18) studied the pretreatment of ion-exchanged $Pt(NH_3)_4^{2+}$ on zeolite HZSM-5 in He and O_2 with UV-Vis spectroscopy and mass spectrometry. For the pretreatment in He, autoreduction was found to occur via the formation of H_2 and N_2 from the NH_3 ligands. Calcination in O_2 led to the production of NO_x in several different steps. The presence of H_2O was found to play a crucial role in the pretreatment, replacing NH_3 as a ligand on the Pt^{2+} complex.

Keegan *et al.* (22) studied calcination and reduction of the same $Pt(NH_3)_4^{2+}$ on a HZSM-5 system using energy-dispersive extended X-ray absorption fine structure (EXAFS). They showed that during calcination the Pt–Pt coordination rises, indicating agglomeration. The final metal-particle size obtained after direct reduction (no calcination prior to the reduction) was smaller than the particle size obtained after calcination prior to the reduction. The authors did not clarify the chemistry of the pretreatment process.

All these reports mainly deal with exchanged $Pt(NH_3)_4^{2+}$ on zeolite. The main difference between exchanged and impregnated $[Pt^{2+}(NH_3)_4](NO_3^-)_2$ is the presence of nitric groups (NO_3^-) on the support in the impregnated case. As will be shown, these groups play a vital role in pretreatment of the impregnated catalyst precursor.

An example of a study that deals with impregnated $[Pt^{2+}(NH_3)_4](NO_3^-)_2$ on silica is the study by Zou and Gonzalez (23). Using *in situ* UV reflectance spectroscopy, they establish the presence of the same mobile $Pt(NH_3)_2H_2$ hydride in the same temperature range as Dalla Betta and Boudart (21) suggested.

Muñoz-Páez and Koningsberger (24) used a combination of temperature-programmed reduction, MS, and EXAFS to study the decomposition of $[Pt^{2+}(NH_3)_4](OH^-)_2$ impregnated on γ-Al_2O_3. They report the decomposition of the precursor to $Pt(NH_3)_2O$ during drying in He at 120°C and a partial reduction of the precursor to metallic Pt when reduced at 180 and 200°C.

All in all, little has been reported on the reactions taking place for impregnated $[Pt^{2+}(NH_3)_4](NO_3^-)_2$ on macroporous supports. Moreover, the relation of pretreatment to the final particle-size distribution is rarely investigated. In our view, knowledge of the reactions occurring during pretreatment is a crucial step towards the development of a process leading to uniform, small particle sizes.

In this study, a powerful combination of high-resolution transmission electron microscopy (HRTEM), MS, and quick EXAFS (QEXAFS) is used to study the reactions of $[Pt^{2+}(NH_3)_4](NO_3^-)_2$ impregnated on SiO_2 during different pretreatment processes.

MS is used to monitor which gases are produced during pretreatment. QEXAFS is used to study the local structure of the Pt complex during pretreatment. The time scale of QEXAFS scans (30–90 s per scan) is suitable for studying reactions such as pretreatment processes. The white-line area gives information concerning the oxidation state (25). The EXAFS region represents the geometrical structure of the Pt atom. The final metal-particle size was obtained from the Pt–Pt first shell coordination number, hydrogen chemisorption (26), as well as HRTEM.

$[Pt^{2+}(NH_3)_4](NO_3^-)_2$-impregnated SiO_2 was heated in three different gases: an inert gas (Ar or He), H_2, and O_2. As mentioned above, heating in an inert gas leads to autoreduction of the $[Pt^{2+}(NH_3)_4](NO_3^-)_2$ complex. Heating in H_2 leads to a direct reduction of the complex. Heating in O_2 (calcination), generally performed to decompose the complex before reducing the metal, results in the formation of PtO_x.

EXPERIMENTAL

Catalyst Precursor Preparation

Five grams of vacuum-dried SiO_2 (Engelhard, BET surface area 400 m^2/g, pore volume 1.1 ml/g) was impregnated with 5.5 ml of an aqueous solution of $[Pt^{2+}(NH_3)_4](NO_3^-)_2$ (Aldrich, 18.0 mg/ml, resulting in 1 wt% Pt/SiO_2) using the incipient wetness method. The impregnated support was dried in a water-free nitrogen flow for 1 h at room temperature and for 18 h at 80°C.

Pretreatments

Three different pretreatments were performed and studied by both QEXAFS and MS. During each pretreatment the impregnated support was heated in one gas with a

ramp of 2°C/min from room temperature to 400°C. The gases used were (1) either He (QEXAFS) or Ar (MS) (this sample is called Pt[Ar/He]), (2) O_2 (Pt[O_2]), and (3) H_2(Pt[H_2]).

Mass Spectrometry

A continuous down-flow, fixed-bed reactor (inner diameter 0.8 cm) was loaded with a sieve fraction (212 μm < d_p < 425 μm) of 1 g of the impregnated SiO_2. The outlet of the reactor was connected to a quadrupole mass spectrometer (Balzers QMS 420) via a capillary. The monitored masses (ions) were 2 (H_2^+), 16 (NH_2^+, O^+), 17 (NH_3^+, OH^+), 18 (H_2O^+), 28 (N_2^+), 30 (NO^+), 32 (O_2^+), 40 (Ar^+), 44 (N_2O^+), and 46 (NO_2^+) amu. With these masses, all likely reaction products can be monitored. Mass 16 was used to identify NH_3 since the contribution of the O^+ fragment ion of H_2O is limited for this mass and can easily be corrected for.

Quick EXAFS

Impregnated SiO_2 (120 mg) was pressed in a self-supporting wafer and mounted in a stainless steel *in situ* cell (27). This cell was attached to a series of flow controllers and to a temperature controller. It was checked that differences between the layout of the *in situ* EXAFS cell and the down-flow reactor used for the MS experiments do not result in differences in temperature profiles and reactions of the catalyst precursor.

QEXAFS measurements were performed at the HASYLAB synchrotron (station X1.1) in Hamburg, Germany. The measurements were done in transmission mode using ion chambers filled with a mixture of Ar and N_2, with an absorption of 20% in the first and 80% in the second ionisation chamber. The monochromator [a double Si(111) crystal] was detuned to 50% at maximum intensity to avoid the presence of higher harmonics in the X-ray beam. In QEXAFS mode, the monochromator is in continual motion.

The QEXAFS scans were performed at the Pt L_3 edge (11,564 eV) and were taken from 11,500–12,000 eV with steps of 1 eV. Each 60 s one scan was taken.

The absorption data was background-subtracted using standard procedures (28, 29). The spectra were normalised on the height of the edge-step at 50 eV over the edge. The white-line intensity was determined by the height of the white-line after normalisation. Data analysis was performed by multiple shell fitting in R-space (1.3 < R < 3.2 Å, 2.5 < k < 9.5 Å^{-1}). k-weightings of 1 and 2 were used. Calibrated theoretical references (30) obtained with FEFF7 (31) were used as references. The references can be used for $k > 2.5$ Å^{-1}. The variances in imaginary and absolute parts were used to determine the fit quality (29). Different backscatterers were identified by applying the difference-file technique (32) using phase-corrected Fourier transforms.

Transferability of the phase shift and amplitude among the nearest neighbours for the whole periodic table is generally assumed (25). Using EXAFS no distinction between nitrogen and oxygen neighbours can therefore be made and nitrogen neighbours are analysed using a Pt–O reference compound.

Hydrogen Chemisorption

Experimental details of hydrogen chemisorption measurements are described elsewhere (33). Typically, the reduced samples are evacuated at 200°C and the hydrogen uptake is measured at 35°C.

The samples were prepared *in situ* from the starting material using the same pretreatments as described above. The sample heated in He (Pt[Ar/He]) was measured twice: once directly after the pretreatment and once after the sample had been flushed with H_2 at 400°C for 30 min following the autoreduction before it was cooled down to measure the hydrogen chemisorption. This was done to check whether all platinum was reduced after autoreduction. The sample heated in O_2 (Pt[O_2]) was subsequently also flushed at 400°C with He and H_2 to reduce the Pt particles prior to chemisorption measurement.

Transmission Electron Microscopy

For samples Pt[Ar/He] and Pt[H_2] several pictures were recorded. For both samples the size of over 230 Pt particles on the pictures was measured. This was used to determine the average metal-particle size and the distribution in particle size. The limit in particle size for detection with HRTEM of the Pt particles is 5–10 Å (i.e, smaller particles are invisible).

HRTEM was performed by the Dutch National Centre for high-resolution electron microscopy. The microscope was a Philips CM30T transmission electron microscope with a LaB_6 filament operating at 300 kV. Samples were mounted on a microgrid carbon polymer supported on a copper grid by placing a few droplets of a suspension of ground sample in ethanol on the grid, followed by drying at ambient conditions.

RESULTS

Direct Reduction, Pt[H_2]

Table 1 summarises the results for hydrogen chemisorption, HRTEM, and EXAFS analysis for all samples.

In Fig. 1, the development of the normalised near-edge region of the Pt L_3 edge during heating is shown. A sharp decrease in the white-line intensity between 150 and 200°C is observed.

The EXAFS region of the QEXAFS spectra was analysed. In Fig. 2, an example is given of the Fourier transform and its best R-space fit of the spectrum taken at 50°C. The fit

TABLE 1

Sample Properties

Sample	H/Pt[a] Total	H/Pt[a] Strong	HRTEM [diameter (Å)]	Final[b] coordination number Pt–O	Final[b] coordination number Pt–Pt
$Pt(H_2)$	0.89	0.36	18	0.2	9.5
Pt(He/Ar) I[c]	0.99	0.39	14	0.0	7.8
Pt(He/Ar) II[d]	1.09	0.53			
$Pt(O_2)$	0.80[e]	0.30	n.d.	3.7	0

[a] The margin of error in the H/Pt value is approximately ±0.03.

[b] The final coordination numbers were derived from the QEXAFS spectrum at 400°C. The initial (at 50°C) Pt–O(N) coordination number was in all cases 5.0–5.4. The initial Pt–Pt coordination number was in all cases 0.

[c] Hydrogen chemisorption was measured directly after autoreduction.

[d] The autoreduction was followed by reduction for 30 min in H_2 at 400°C.

[e] Hydrogen chemisorption was determined for Pt(He/Ar) after reduction at 400°C for 60 min following calcination.

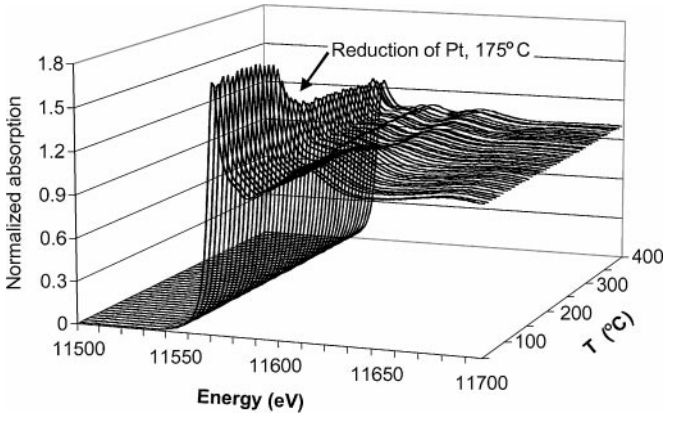

FIG. 1. The near-edge region of the Pt L_3 edge during heating of $[Pt^{2+}(NH_3)_4](NO_3^-)_2$ on SiO_2 in H_2. The sharp decrease between 150 and 200°C indicates reduction of the Pt.

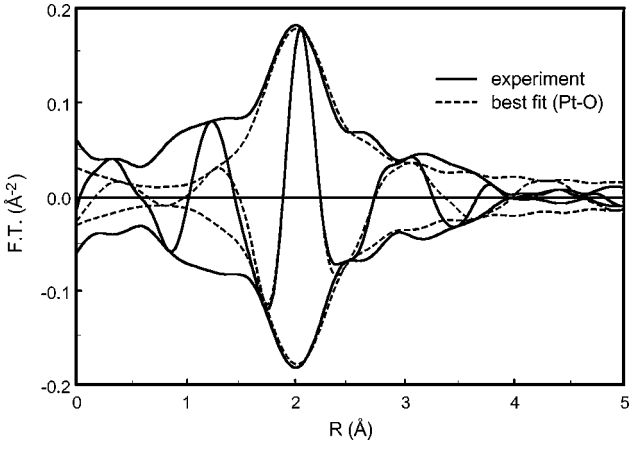

FIG. 2. An example of a Fourier transform and best-fit (R-space fit, single Pt–O shell, $1.3 < R < 2.6$ Å, k^1 weighted, $2.5 < k < 9.5$ Å^{-1}) based on a QEXAFS spectrum obtained during heating in H_2 at 50°C.

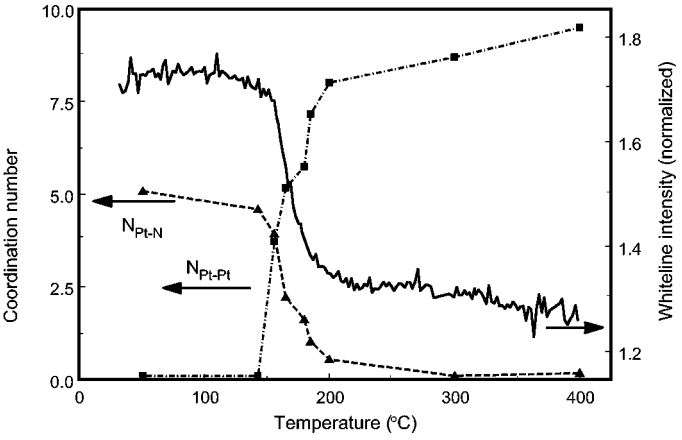

FIG. 3. The normalised white-line intensity (solid line), the Pt–N coordination number (broken line, triangles), and the Pt–Pt coordination number (broken–dotted line, boxes) as a function of temperature during heating of $Pt(NH_3)_4(NO_3)_2$ on SiO_2 in H_2.

was performed with a Pt–O reference. It is noted again that no distinction between O and N neighbours can be made. The fit and experiment are in good agreement. This quality of the experimental data and of the fit is representative for all spectra. This spectrum represents the freshly impregnated $[Pt^{2+}(NH_3)_4](NO_3^-)_2/SiO_2$. The Pt–Pt coordination number is 0, as expected, and the fitted Pt–N coordination number is 5.1.

In Fig. 3, the white-line intensity and Pt–Pt and Pt–N coordination numbers as a function of temperature are shown. All fit parameters are given in Table 2. From Fig. 3 it is obvious that the white-line intensity sharply decreases for $150°C < T < 200°C$, in a temperature range of only 50°C. This is accompanied by a simultaneous decrease in Pt–N coordination number and increase in Pt–Pt coordination number. The Pt–Pt coordination number rises from 0 at 150° to 8.0 at 200°C. The final Pt–Pt coordination number at 400°C is 9.5. The Pt–N coordination number drops from 4.6 at 150°C to 0.5 at 200°C.

Figure 4 shows the intensity of masses 16 (ions NH_2^+, O^+), 17 (NH_3^+, OH^+), and 18 (H_2O^+) during heating of the catalyst precursor in H_2. No other gases are produced.

Below 100°C, the desorption of physisorbed H_2O is observed. Around 210°C a clear maximum in the desorption of H_2O and NH_3 is observed. Although mass 16 is caused by fragment ions of H_2O and NH_3, the intensity of mass 16 is too high to be explained by H_2O only. Therefore, it must be concluded that NH_3 desorbs simultaneously. A strong shoulder in the desorption of H_2O is observed between 150 and 200°C.

Comparing the results presented in Figs. 3 and 4 shows that in the temperature range during which mass spectrometry shows the largest amounts of desorbed gases (maximum at 210°C), QEXAFS shows only minor changes in the Pt complex. Vice versa, in the temperature range in which QEXAFS shows a large change in the local structure

TABLE 2

Fit Parameters[a] of QEXAFS Spectra during Heating in H_2 and Variances of Fits

	O shell				Pt shell				Variances (%)	
T (°C)	R (Å)	N	$\Delta\sigma^{2b}$	E_0	R (Å)	N	$\Delta\sigma^{2b}$	E_0	Im.	Abs.
51[c]	2.01	5.1	4.6	3.4	—[d]	—	—	—	0.595	0.319
143	2.01	4.6	4.3	4.0	—[d]	—	—	—	0.318	0.139
156	2.0	3.3	1.8	4.2	2.71	3.7	14.2	10.0	1.01	0.490
165	1.98	2.2	2.6	6.1	2.68	5.2	11.5	9.0	1.07	0.250
180	1.99	1.6	3.6	4.3	2.70	5.6	9.6	4.9	0.661	0.348
185	1.95	1.0	5.6	10.0	2.70	7.2	10.4	3.9	0.690	0.318
200	1.97	0.5	8.0	10.0	2.70	8.0	10.3	3.4	0.501	0.106
300	—[d]	—	—	—	2.70	8.7	11.8	2.6	0.904	0.605
400	—[d]	—	—	—	2.67	9.5	15.6	2.9	1.25	0.323

[a] Errors in fits: $R \pm 1\%$, $N \pm 20\%$, $\Delta\sigma^2 \pm 5\%$, $E_0 \pm 10\%$. R-space fit: $\Delta k = 2.5 - 9.5$ Å, $\Delta R = 1.3$–3.2 Å, k^2 weighted.

[b] Debye–Waller factor $\times 10^{-3}$, $\pm$.

[c] Fit with k^1 weighting, $1.3 < R < 2.5$ Å.

[d] No contribution of this shell present.

of the Pt, only the desorption of H_2O is observed as a shoulder in the large H_2O signal at 210°C and no other gases are detected.

HRTEM was used to determine the final metal-particle size. A representative photograph is shown in Fig. 5. Multiple photographs were analysed and the size of at least 230 particles was measured to determine the average particle size and the particle-size distribution (Fig. 6, bars filled with bricks). The particle-size distribution appears to be bimodal, with maxima at 14 and 22 Å. The average particle size (as determined by HRTEM) for this sample is 18 Å.

Hydrogen chemisorption showed an average hydrogen coverage of $H_{total}/Pt = 0.89$ (Table 1).

Autoreduction, Pt[Ar/He]

In Table 1, the results for hydrogen chemisorption, HRTEM, and EXAFS analysis are given.

Heating the sample in Ar leads to the desorption of various gases, which are probed with mass spectrometry (Fig. 7). Below 100°C, physisorbed H_2O desorbs as shown by the desorption of masses 18, 17, and 16. Further heating leads to the desorption of NO_x, H_2O, NH_3, and N_2 in two temperature ranges. First, in a broad peak around 210°C the desorption of NO_x, H_2O, NH_3, and N_2 is observed. At a temperature of 240°C a second, sharper desorption peak for the same gases is observed. In the whole temperature range the desorption of NO_2, O_2, and H_2 is not detected.

The QEXAFS results are given in Fig. 8 and Table 3. Heating the sample in He first shows a small increase in the white line from 180 to 200°C, accompanied by a decrease in the Pt–N coordination number. A sharp decrease from 1.7 to 1.4 in the white-line intensity starts at 200°C and continues up to approximately 260°C, after which the white line continues to decrease slowly until the highest temperature

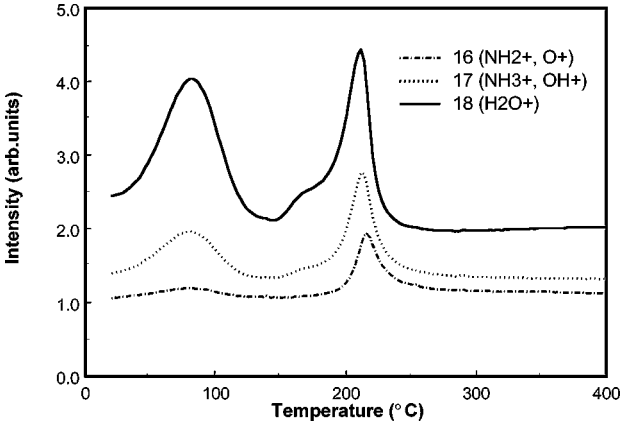

FIG. 4. The intensity of (fragment) ions of desorbed gases vs temperature during reduction in H_2.

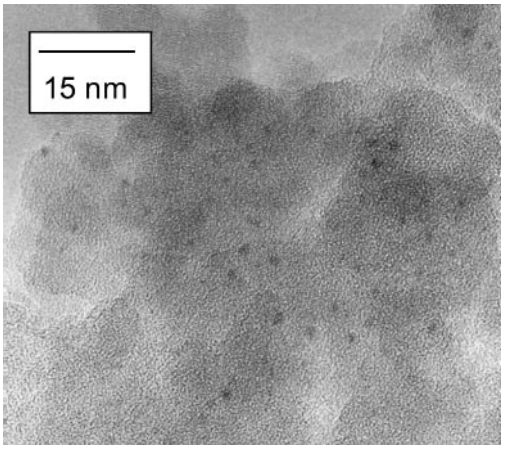

FIG. 5. A representative HRTEM picture of the sample after direct reduction (Pt[H_2]). Dark spots: Pt particles.

TABLE 3

Fit Parameters[a] of QEXAFS Spectra during Heating in He and Variances of Fits

	O shell				Pt shell				Variances (%)	
T (°C)	R (Å)	N	$\Delta\sigma^{2b}$	E_0	R (Å)	N	$\Delta\sigma^{2b}$	E_0	Im.	Abs.
50[c]	2.01	5.4	6.2	4.6	—[d]	—	—	—	0.044	0.012
150[c]	2.00	5.4	6.0	4.9	—	—	—	—	0.108	0.019
197[c]	1.99	4.4	3.3	5.3	—	—	—	—	0.371	0.095
209[c]	1.99	3.9	5.8	4.7	—	—	—	—	0.322	0.129
220	2.01	3.2	8.4	2.6	2.59	2.3	14.4	10.0	1.720	0.222
234	1.94	3.1	12.6	9.3	2.63	5.7	17.3	9.2	0.979	0.407
249	1.97	0.6	6.8	6.6	2.65	6.6	18.4	7.4	0.448	0.146
300	1.94	1.7	25.0	10.0	2.68	7.7	15.9	3.7	1.92	1.02
400	2.19	0.5	5.0	9.9	2.61	7.8	16.9	3.9	3.95	1.61

[a] Errors in fits: $R \pm 1\%$, $N \pm 20\%$, $\Delta\sigma^2 \pm 5\%$, $E_0 \pm 10\%$. R-space fit: $\Delta k = 2.5$–9.5 Å, $\Delta R = 1.3$–3.2 Å, k^2 weighted.

[b] Debye–Waller factor $\times 10^{-3}$.

[c] Fit was done with k^1 weighting, with $1.3 < R < 2.5$ Å.

[d] No contribution of this shell present.

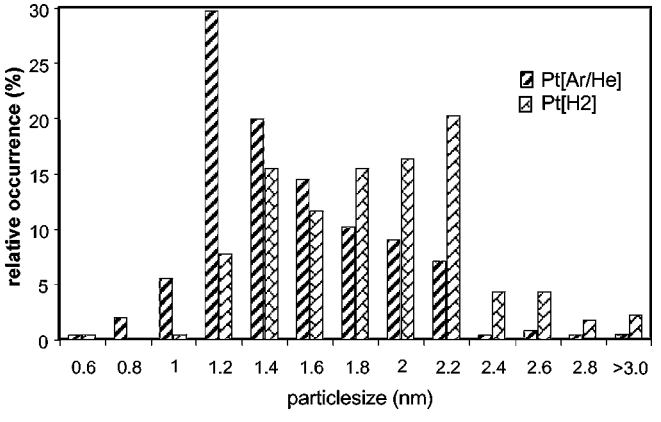

FIG. 6. The particle-size distribution as determined by HRTEM by measuring the size of >230 particles. Bar filled with lines: autoreduced sample (Pt[Ar/He]). Bricks: directly reduced sample (Pt[H_2]).

measured (400°C). The sharp decrease in the white line between 200 and 260°C is accompanied by a sharp decrease in the Pt–N coordination number from approximately 4.5 to 2 and an increase in the Pt–Pt coordination number from 0 to approximately 7. At higher temperatures, the nitrogen neighbours disappear slowly and the Pt–Pt coordination shows no significant changes.

Hydrogen chemisorption (Table 1) for this sample without an additional high temperature reduction shows a H_{total}/Pt value of 0.99. The additional high temperature reduction leads to an increase in H_{total}/Pt to 1.09.

In Fig. 6 the particle-size distribution for this sample as determined by HRTEM is shown (bars filled with lines). The average particle size for this sample is 14 Å. Compared to that of sample Pt[H_2], the particle-size distribution is

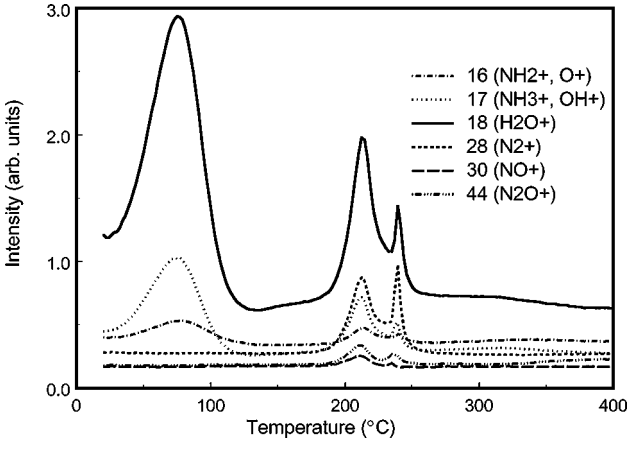

FIG. 7. The intensity of (fragment) ions of desorbed gases vs temperature during heating in Ar.

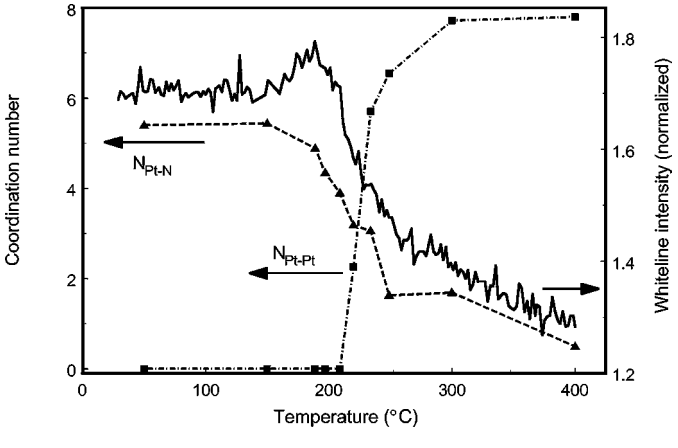

FIG. 8. The normalised white-line intensity (solid line), the Pt–N coordination number (broken line, triangles), and the Pt–Pt coordination number (broken–dotted line, boxes) as a function of temperature during heating of $[Pt^{2+}(NH_3)_4](NO_3^-)_2$ on SiO_2 in He.

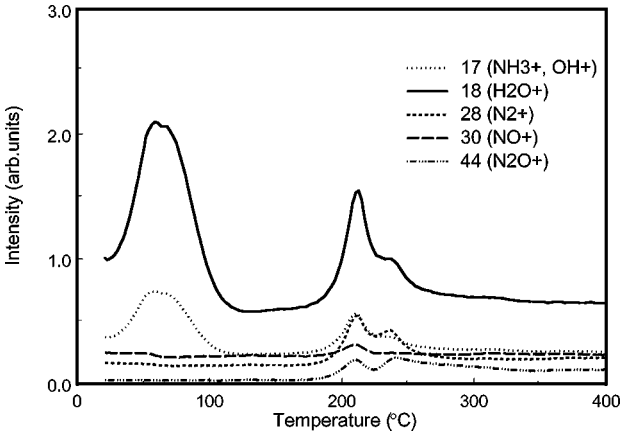

FIG. 9. The intensity of (fragment) ions of the desorbed gases vs temperature during calcination in O_2.

more uniform, with only one maximum at 12 Å and 50% of the particles in the range of 12–14 Å.

Calcination, Pt[O_2]

Calcination of the impregnated sample in O_2 again shows the desorption of physisorbed H_2O below 100°C (Fig. 9). Similarly to heating the impregnated sample in Ar, heating the sample in O_2 leads to the desorption of NO_x, H_2O, NH_3, and N_2 at 2 temperatures, viz. at 210 and 240°C. NO_2 and H_2 were not detected. NH_3 could not be identified through its fragment ion NH_2^+ because the O_2 in the gas flow leads to high quantities of O^+ with mass 16.

QEXAFS (Fig. 10) shows an increase in the white-line intensity between 150 and 325°C from 1.7 to 2.05. This increase is accompanied by a decrease in the Pt–O coordination number from 5.3 to 4.0 (see also Table 4). During the entire calcination procedure, no Pt–Pt neighbours are observed.

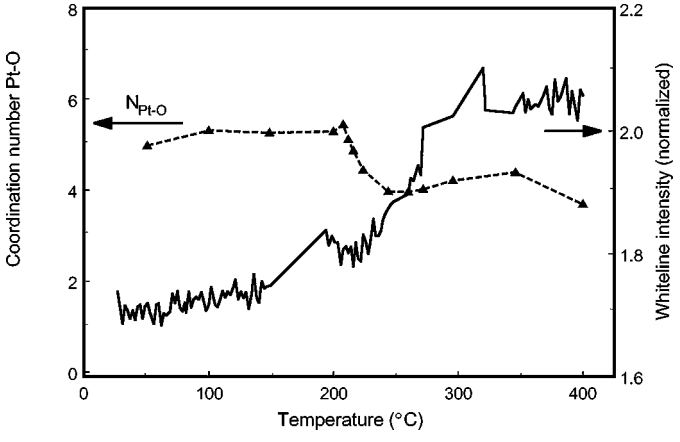

FIG. 10. The normalised white-line intensity (solid line) and the Pt–O coordination (broken line, triangles) vs temperature during heating of $[Pt^{2+}(NH_3)_4](NO_3^-)_2$ on SiO_2 in O_2. No Pt–Pt coordination was observed.

TABLE 4

Fit Parameters[a] of QEXAFS Spectra during Heating in O_2 and Variances of Fits

	O shell				Variances (%)	
T (°C)	R (Å)	N	$\Delta\sigma^2(10^{-3})$	E_0	Im.	Abs.
51	2.00	5.0	3.8	4.6	0.197	0.159
100	2.00	5.3	5.2	5.0	0.111	0.106
149	2.01	5.3	5.3	4.5	0.346	0.254
200	1.99	5.3	6.3	5.5	0.277	0.227
208	1.97	5.4	7.9	6.3	0.110	0.075
212	1.98	5.1	7.1	6.0	0.158	0.060
216	1.98	4.9	7.5	5.4	0.116	0.037
224	1.98	4.4	6.5	4.6	0.122	0.016
244	1.98	4.0	5.0	5.4	0.259	0.125
260	1.98	4.0	4.3	5.8	0.238	0.068
272	1.99	4.0	3.7	4.8	0.268	0.119
296	1.98	4.2	4.9	5.1	0.932	0.588
346	1.98	4.4	4.4	5.5	0.508	0.268
400	2.01	3.7	3.0	1.7	0.898	0.749

[a] Errors in fits: $R \pm 1\%$, $N \pm 20\%$, $\Delta\sigma^2 \pm 5\%$, $E_0 \pm 10\%$. R-space fit: $\Delta k = 2.5$–9.5 Å, $\Delta R = 1.3$–2.5 Å, k^1 weighted.

Hydrogen chemisorption after reduction following the calcination resulted in $H_{total}/Pt = 0.80$ (Table 1).

DISCUSSION

Reliability of Results from QEXAFS and HRTEM

In a QEXAFS experiment, the monochromator is in continual motion. Accompanied by the low counting (120 ms) time per data-point, this gives a relatively low signal-to-noise ratio. This is most significant at higher energies since the amplitude of the EXAFS-wiggles decreases at higher energies. As a consequence, the measured QEXAFS spectra are considered only reliable up to $k = 9.5$ Å^{-1}, in contrast to typical EXAFS spectra of Pt-containing compounds, which can be used up to $k = 15$ Å^{-1}. Using the Nyquist theorem (29), the maximum number of free parameters that can be fitted doing a R-space fit of the data ($1.3 < R < 2.9$ Å, $2.5 < k < 9.5$ Å^{-1}) is nine. With nine free parameters two shells (N and Pt) can be fitted. Pt–Pt and Pt–O/N contributions have differences in backscattering-amplitudes, which are most prominent at higher energies. Therefore, fitting and discriminating between Pt and O/N backscatterers is less reliable using QEXAFS compared to normal EXAFS, where typically three spectra up to $k = 15$ Å^{-1} of 30 min each are averaged. Moreover, the samples have temperatures between room temperature and 400°C. At high temperatures the thermal disorder is high. A high disorder leads to additional damping of the EXAFS-wiggles at higher energies. This results in an additional error in the fitting of the QEXAFS spectra. The error in the fitted coordination number is estimated at approximately ±2.

However, all samples are similar (all have the same starting material, loading, and temperature range) and the differences in the sample between consecutive spectra are minimal. Therefore, the *differences* in the structural parameters as observed are reliable even though the absolute values may differ from the true physical parameters.

HRTEM allows the direct measurement of particle sizes larger than 5–10 Å. Depending on contrast, thickness of the sample, and location of the Pt particle on the support, particles smaller then 5–10 Å are invisible. As these particles contain only a few atoms, they consist exclusively of surface atoms. Therefore, these small particles are extremely important in catalysis.

In addition, although these small particles are not probed by HRTEM, hydrogen chemisorption is determined largely using these small particles. Extremely small (<10 Å) Pt particles are known to adsorb more than one hydrogen per Pt (34). This may result in discrepancies between the particle size as determined by HRTEM and hydrogen chemisorption.

Direct Reduction

Direct reduction is characterised by large changes in the Pt-complex between 150 and 200°C. The Pt–Pt coordination increases rapidly while both the Pt–N coordination and white-line intensity decrease (Fig. 3 and Table 2). These changes are characteristic of a reduction in the Pt^{2+} complex and the formation of metal-particles. It is remarkable that in this temperature range only the desorption of a small amount of H_2O is observed (Fig. 4). Only at higher temperatures (210°C), are the desorption of NH_3 and large amounts of H_2O observed. In this region, QEXAFS shows that the reduction is nearly complete. This implies that the gases desorbing at 210°C must be produced by a mechanism independent of the reduction in the Pt^{2+} complex.

A proposed mechanism is shown in Scheme 1. Most likely, during the drying procedure following impregnation, $[Pt^{2+}(NH_3)_4](OH^-)_2$ and HNO_3 are formed in separate regions of the support. Although this may seem an unlikely reaction at first sight, this separation is very conceivable during impregnation. When the metal precursor is dissolved, the $[Pt^{2+}(NH_3)_4](NO_3^-)_2$ complex is dissociated into $Pt(NH_3)_4^{2+}$ and NO_3^-. Impregnation is followed by

$$[Pt^{2+}(NH_3)_4](OH^-)_2 + 2\,HNO_3\,(s) + H_2$$

$$\downarrow \text{150-200°C, } H_2 \qquad (1)$$

$$Pt^0\,(s) + 2\,NH_4NO_3\,(s) + 2\,H_2O\,(g) + 2\,NH_3$$

$$\rightarrow \text{210°C, } H_2 \quad NH_3\,(g) + H_2O\,(g) \qquad (2)$$

SCHEME 1. Proposed mechanism for direct reduction.

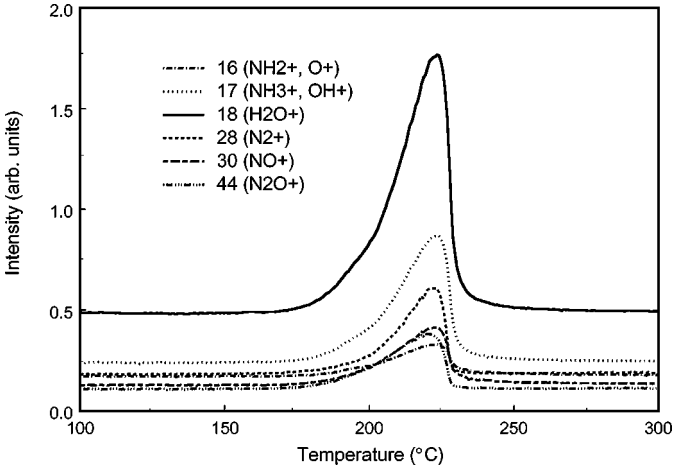

FIG. 11. The decomposition of NH_4NO_3 during heating, followed by MS.

drying the impregnated support. During this drying, NO_3^- is transported to specific places on the support, where the capillary forces are greatest and, hence, water is evaporated last. However, during drying the Pt^{2+} complex remains behind on the SiO_2 surface and, hence, the homogeneous distribution of Pt^{2+} and NO_3^- is distorted and they precipitate as $[Pt^{2+}(NH_3)_4](OH^-)_2$ and HNO_3.

During reduction of the Pt complex, two of the ammonia ligands react with this HNO_3 to form ammonium nitrate, NH_4NO_3. This complex is unstable at higher temperatures and has a boiling point of 211°C. When this complex decomposes, nitric oxides (NO_x) and H_2O are produced (Fig. 11). In a hydrogen atmosphere, NO_x can be reduced to NH_3 and H_2O in the presence of Pt. These gases are indeed observed.

The final particle size as determined by QEXAFS, hydrogen chemisorption, and HRTEM is quite large compared to the autoreduced sample (Table 1). Hydrogen chemisorption shows a H/Pt value of 0.89, with QEXAFS giving a Pt–Pt coordination number of 9.5. Normally, a coordination number of 9.5 would correlate to a H/Pt value of approximately 0.6 (34). However, as described before, the absolute Pt–Pt coordination number based on QEXAFS contains a large margin of error (±2). Based on HRTEM and hydrogen chemisorption, the average metal-particle size is estimated at 14–16 Å.

In addition, the particle-size distribution is broad (Fig. 6). A broad particle-size distribution is typically caused by a sintering process. Directly after the reduction, at 200°C, a high Pt–Pt coordination (~8) number is reached. Apparently, during direct reduction sintering of the metal particles takes place. This is confirmed by the QEXAFS results.

The final metal-particle size is determined by the ratio of two parameters, the growth and nucleation rate (35). If the growth rate is high, the first nuclei will rapidly grow to large particles. Since the formation of metal–metal bonds adds significantly to the stability of Pt atoms (36, 37), the

reduction of the $Pt^{2+}(NH_3)_x$ complex must involve a migration and collision of the Pt^{2+} species with either an earlier formed metallic Pt nucleus or several other Pt^{2+} complexes and reduce at the same moment. The rapid reduction of the Pt^{2+} complex, the high growth-rate of the Pt particles in the temperature range of 150–200°C, as observed with QEXAFS, and the low final dispersion therefore indicate the presence of a highly mobile species during the reduction, able to precipitate on the nucleus. It is very likely that this mobile species is similar to the $[Pt^{\delta+}(NH_3)_2H_2^{\delta-}]^0$ hydride, reported for direct reduction of $Pt(NH_3)_4^{2+}$ on zeolites (21) and SiO_2 (23). However, these hydrides were reported in the temperature range of 60–100°C. In this study, the MS results clearly show that the impregnated complex remains intact up to 150°C.

The sudden formation of large particles above 150°C is in agreement with observations made earlier (23, 24). Muñoz-Páez and Koningsberger (24) studied $[Pt^{2+}(NH_3)_4](OH^-)_2$ on γ-Al_2O_3 and observed a large Pt–Pt coordination number after heating the catalyst in H_2 to 200°C and cooling it down again to liquid nitrogen temperature to perform EXAFS measurements. They did not observe the characteristic H_2O/NH_3 desorption at 211°C, and it was not to be expected since they used $[Pt^{2+}(NH_3)_4](OH^-)_2$ instead of $[Pt^{2+}(NH_3)_4](NO_3^-)_2$.

The results for the data analysis for the QEXAFS scans show some interesting features (Table 2). At lower temperatures, with a high amount of nitrogen neighbours, the E_0 for the Pt–N reference is 3.4 and the E_0 for the Pt–Pt reference is 10.0. At higher temperatures, with mainly metallic platinum particles, the situation is reversed: the E_0 for the Pt–N reference is high (10.0) and the E_0 for the Pt–Pt reference is low (2.9). This resembles a change in the edge from Pt^{2+} to Pt^0. Furthermore, in the early stages of the reduction the Debye–Waller factor for the Pt–Pt coordination is large (14.2×10^{-3}) and this drops to 9.6×10^{-3}. Then, when the reduction is nearly complete, the Debye–Waller factor increases again (to 15.6×10^{-3}). The initial decrease of the Debye–Waller factor is caused by the formation of larger particles, which are structurally more ordered than are smaller particles. The subsequent increase in the Debye–Waller factor is caused by the increase in temperature, which results in a higher thermal disorder. In conclusion, the direct reduction is a fast process taking place between 150 and 200°C, resulting in relatively large particles with an average size of 14–16 Å and a bimodal particle-size distribution. The desorption of NH_3 and H_2O at 211°C is caused by the decomposition of NH_4NO_3 in an independent process of the reduction.

Autoreduction

The decrease in the white line when high temperatures are compared to low temperatures (QEXAFS, Fig. 8) indicates an autoreduction of the Pt^{2+} complex. The observation that autoreduction takes place is in agreement with observations made in the literature (18). The process of autoreduction is characterised by slow reduction of the Pt^{2+} complex (starting at 200°C) and the relatively low final metal-particle size (Table 1), as the H/Pt number of 1.09 shows.

A peculiar observation is made with QEXAFS (Fig. 8). The white line shows a small increase from 175–200°C. Simultaneously, the number of nitrogen neighbours decreases. This can be explained as follows: Each NH_3 ligand will donate some electron density to the Pt^{2+} ion via the nitrogen lone pair. When a NH_3 ligand is desorbed, overall less electron density is donated to the Pt^{2+}. This results in an increase in the number of holes in the d-orbitals, which in turn results in higher white-line intensity. Therefore, the conclusion is that at least one ammonia group is desorbed from the Pt^{2+} between 175 and 200°C. However, mass spectrometry shows that no gases are produced until 200°C. This means that the desorbed NH_3 remains in the sample. It is likely that it reacts with HNO_3 to precipitate as NH_4NO_3(reaction 3, Scheme 2). This mechanism is similar to the mechanism proposed for direct reduction. NH_4NO_3 is unstable at higher temperatures, forming nitric oxides and H_2O. Indeed, mass spectrometry shows the production of N_2, O_2, NO_x, H_2O, and some NH_3 between 200 and 250°C, with maximum intensity at 211°C (Fig. 7) and a second maximum at 240°C.

Simultaneously to the desorption of these gases, QEXAFS shows a large decrease in the white line in the temperature range of 200–250°C. In addition, the Pt–Pt coordination number increases from 0 to ~6 while the Pt–N coordination number decreases from 5 to 1.5. This implies that the Pt complex is reduced to a great extent in this temperature range. In the preceding paragraph (direct reduction), it was shown that production and decomposition of NH_4NO_3 is not necessarily coupled to the reduction of the Pt^{2+} complex. However, the gases produced during the decomposition might very well influence the Pt^{2+} complex. This is apparent when the first derivative of the white line as a function of temperature is compared with the desorption of H_2O (Fig. 12). The decrease in the white line is maximal

$$[Pt^{2+}(NH_3)_4](OH^-)_2 + HNO_3 \xrightarrow{175\text{-}200^\circ C} Pt^{2+}(NH_3)_3(OH^-)_2 + NH_4NO_3 \quad (3)$$

$$Pt^{2+}(NH_3)_3(OH^-)_2 + NH_4NO_3 \xrightarrow{210^\circ C} N_2O, NO, H_2O, NH_3 \quad (4)$$

$$Pt^{2+}(NH_3)_3(OH^-)_2 + 2/x\ NO_x \xrightarrow{210, 240^\circ C} Pt^0 + 4\ H_2O + 1/x\ N_2 + NH_3 \quad (5)$$

$$Pt^{2+}(NH_3)_x(OH^-)_2 \xrightarrow[Pt^0]{250\text{ - }400^\circ C} Pt^0 + 2\ H_2O + (x\text{-}1)\ NH_3 + \tfrac{1}{2}\ H_2 + \tfrac{1}{2}\ N_2 \quad (6)$$

SCHEME 2. Proposed mechanisms taking place during autoreduction.

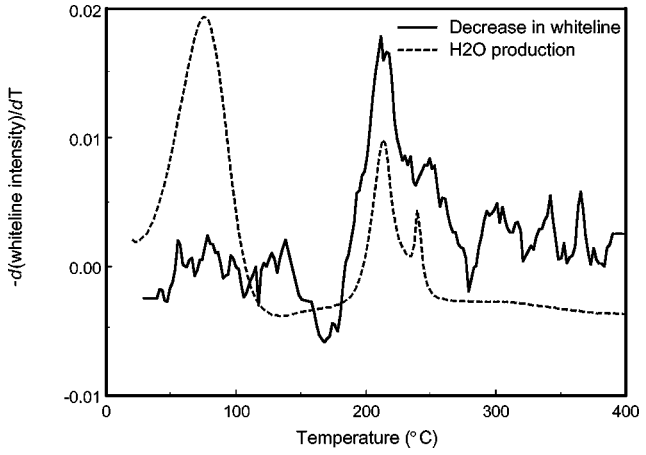

FIG. 12. The decrease in the white-line (first derivative, solid line) and the production of H_2O (dotted line) vs temperature during heating impregnated $[Pt^{2+}(NH_3)_4](NO_3^-)_2/SiO_2$.

when the highest amount of gases is produced, and vice versa, with the highest reduction rate at 210°C, and a second maximum at approximately 240–250°C. This confirms that reduction must be influenced by the gases produced during the decomposition of NH_4NO_3, either NH_3 or NO_x (reaction 4, Scheme 2). Since the Pt complex already has a high amount of NH_3 ligands, it is most likely that the NO_x influences the reduction. A mechanism for this reduction is proposed in reaction 5, Scheme 2.

At temperatures higher than 250°C, the reduction continues gradually, as is indicated by the decrease in the white-line (Fig. 8). The Pt–O (N) coordination number (CN = 1.5) at 250°C is still relatively high and decreases slowly. This indicates that not all Pt^{2+} complexes are reduced by the NO_x and another reduction mechanism takes over: autoreduction. This autoreduction is characterised by the reduction of Pt^{2+} to Pt^0 accompanied by a loss of ligands. No other molecules are involved in the reduction. The proposed mechanism is given in reaction 6, Scheme 2. This reaction is similar to the one proposed by van den Broek *et al*. (18). A major difference between their study and the present one is in the support material: They use the zeolite ZSM5; in this study SiO_2 is used. With this acidic zeolite, any NH_3 adsorbs strongly on the Brønsted acidic sites, whereas on SiO_2 NH_3 desorbs from the silanol surface groups below 100°C. The presence of NH_3 in zeolites at higher temperatures can lead to the formation of the highly mobile $Pt(NH_3)_2H_2$ hydrides, leading to sintering (18).

The slow rate of reduction of the complex is probably due to kinetic reasons. As discussed in the previous paragraph (direct reduction), the final particle size is governed by the ratio of the growth-rate and nucleation rate (35–38). If the Pt^{2+} complex is not mobile, reduction will be extremely slow and the final metal-particle size will be small.

At 400°C, the white line is still decreasing, indicating that reduction is still not complete. This is confirmed by the hydrogen chemisorption experiments. The autoreduction followed by an additional reduction in H_2 for 30 min at 400°C results in higher hydrogen uptake (H/Pt = 1.09, Table 1) compared to the autoreduced sample without additional reduction (H/Pt = 0.99). The lower hydrogen uptake indicates that not all Pt is in the reduced state, since admission of hydrogen at 35°C does not result in a reduction of the Pt complex.

All techniques reveal a smaller average particle size after autoreduction than after direct reduction. The high H/Pt number (1.09, Table 1) for the autoreduced sample shows that the final metal-particle size is very small. According to Kip *et al.* (34), and assuming spherical particles, this H/Pt value corresponds to an average diameter of approximately 10–12 Å, with particles consisting of approximately 20 Pt atoms. This is in agreement with the upper limit of the average particle size of 14 Å, as determined by HRTEM. The particle-size distribution is significantly narrower than in the case of the directly reduced sample (see Fig. 6). EXAFS gives a Pt–Pt coordination number of approximately 7.5.

In conclusion, heating the catalyst precursor in an inert atmosphere leads to a multiple-step reduction, involving reduction by NO_x and autoreduction. The final metal-particle size is approximately 10–12 Å and the metal-particles are relatively uniform.

Calcination

In Table 1, the results of hydrogen chemisorption, HRTEM, and EXAFS analysis are given for this pretreatment.

QEXAFS during the calcination (Fig. 10) shows a constant number of oxygen (or nitrogen) neighbours up to 200°C. This higher stability of $[Pt^{2+}(NH_3)_4](NO_3^-)_2$ in O_2 compared to the stability in H_2 is in agreement with the observations of Kinoshita *et al.* (20). As expected during calcination, no metallic Pt–Pt contribution is present for the whole temperature range. Around 80°C, the white-line starts to increase at a slow rate, although the number of direct Pt–O(N) neighbours remains nearly constant. At present, no clear explanation exists.

Since the oxygen-containing atmosphere gives a high intensity for its fragment ion, O^+ ($m/z = 16$), it was impossible to identify desorbing ammonia by its fragment ion, NH_2^+ ($m/z = 16$). However, it is likely that NH_3 desorbing from Pt^{2+} reacts similarly, as was observed during direct- and autoreduction: it reacts with HNO_3 on the support giving NH_4NO_3 (reaction 7, Scheme 3). The decomposition of NH_4NO_3 (reaction 8, Scheme 3) causes the characteristic broad desorption profile of nitric oxides and water (Fig. 9), with maxima at 210 and 240°C.

The sharp decrease in the Pt–N(O) coordination number and increase in the white-line (Fig. 10) between 200 and 250°C indicates a change in the ligands of the Pt. Probably,

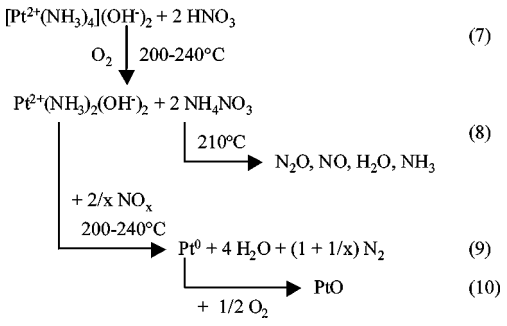

SCHEME 3. Proposed mechanisms taking place during calcination.

the formed NO_x reacts with the Pt^{2+} complex to give Pt^0 (reaction 9, Scheme 3) in a manner similar to that during the autoreduction. Naturally, the formed Pt^0 is immediately oxidised to PtO (reaction 10, Scheme 3).

The final metal-particle size, determined after reduction following the calcination, is large, as is indicated by the H/Pt ratio of 0.80. It is uncertain whether the final dispersion is determined during the calcination or during the subsequent reduction. However, the fast rate of oxidation, as indicated by the sharp increase in the white line and sudden change to PtO_x around 200–250°C, suggests a large growth-rate of PtO_x particles. Probably, the PtO_x particles have the ability to sinter and form large particles (39).

The Final Metal-Particle Size: Processes Leading to Narrow Particle-Size Distributions

Hydrogen chemisorption, HRTEM, and QEXAFS all show that final particle size is smallest after autoreduction. During autoreduction, the reduction proceeds in several steps. Two steps (at 210 and 240°C) show a high reduction rate accompanied by sintering. During this sintering, metal particles in the range of 10–12 Å are formed. The reduction is caused by the formation of NO_x species. A third step, at $T > 250$°C, is the autoreduction of the $Pt^{2+}(NH_3)_x$ complex. This is a slow process, indicating that this species is not mobile. The size of the metal particles appears to be stable during this slow autoreduction.

During direct reduction, the creation of a mobile species at ~150°C results in large Pt particles. In addition, calcination–reduction at higher temperatures leads to the formation of larger Pt particles. QEXAFS shows that PtO_x is formed after calcination. It is most likely that also PtO_x particles have the ability to sinter (39) and ultimately form larger Pt particles.

The key to making uniform small particles is to have a slow reduction process involving stable, immobile species. Analysis of the particle-size distribution (Fig. 6) shows that Pt[Ar/He] has a narrow particle-size distribution compared to Pt[H_2] and has smaller particles. The disadvantage during autoreduction is the multiple-step reduction. If the presence of NO_x can be removed before pretreatment, the final metal-particle size might be even smaller. One possibility for achieving this might be using $[Pt^{2+}(NH_3)_4](OH^-)_2$ as a precursor.

CONCLUSION

By combining mass spectrometry and *in situ* QEXAFS, it was possible to elucidate the mechanisms taking place during reduction, autoreduction, and calcination of $[Pt^{2+}(NH_3)_4](NO_3^-)_2$ impregnated on SiO_2. The combination of mass spectrometry with QEXAFS showed that the production of gases can be a mechanism independent of the reduction of the $[Pt^{2+}(NH_3)_4](NO_3^-)_2$ precursor.

The smallest particles with the narrowest particle-size distribution are obtained using autoreduction. The key to making small particles is to avoid the formation of mobile species that are able to precipitate as metal clusters.

ACKNOWLEDGMENT

The European Union program for Large Scale Facilities (contract ERBFMGECT950059) is acknowledged for financial support.

REFERENCES

1. Schwarz, J. A., Contescu, C., and Contescu, A., *Chem. Rev.* **95**, 477 (1995).
2. Komiyama, M., *Catal. Rev.–Sci. Eng.* **27**, 341 (1985).
3. Zou, W., and Gonzalez, R. D., *Catal. Lett.* **12**, 73 (1992).
4. Anderson, J. B. F., Burch, R., and Cairns, J. A., *J. Catal.* **107**, 351 (1987).
5. Besoukhanova, C., Guidot, J., and Barthomeuf, D., *J. Chem. Soc., Faraday Trans. 1* **77**, 1595 (1981).
6. Koningsberger, D. C., de Graaf, J., Mojet, B. L., Ramaker, D. E., and Miller, J. T., *Appl. Catal. A* **191**, 205 (2000).
7. Mojet, B. L., Miller, J. T., Ramaker, D. E., and Koningsberger, D. C., *J. Catal.* **186**, 373 (1999).
8. Lietz, G., Lieske, H., Spindler, H., Hanke, W., and Völter, J., *J. Catal.* **81**, 17 (1983).
9. Shelimov, B. N., Lambert, J.-F., Che, M., and Didillon, B., *J. Catal.* **185**, 462 (1999).
10. Shelimov, B. N., Lambert, J.-F., Che, M., and Didillon, B., *J. Mol. Catal. A* **158**, 91 (2000).
11. Regalbuto, J. R., Navada, A., Shadid, S., Bricker, M. L., and Chen, Q., *J. Catal.* **184**, 335 (1999).
12. Reyes, P., Oportus, M., Pecchi, G., Frety, R., and Moraweck, B., *Catal. Lett.* **37**, 193 (1996).
13. Bokhimi, A. A., Novaro, O., Lopez, T., and Gomez, R., *J. Phys. Chem.* **99**, 14403 (1995).
14. Aramendia, M. A., Benítez, J. A., Borau, V., Jimenez, C., Marinas, J. M., Ruiz, J. R., and Urbano, F., *Langmuir* **15**, 1192 (1999).
15. Fiddy, S. G., Newton, M. A., Dent, A. J., Salvini, G., Corker, J. M., Turin, S., Campbell, T., and Evans, J., *Chem. Commun.* **851** (1999).
16. Persaud, L., Bard, A. J., Campion, A., Fox, M. A., Mallouk, T. E., Webber, S. E., and White, J. M., *Inorg. Chem.* **26**, 3825 (1987).
17. Mojet, B. L., Ramaker, D. E., Miller, J. T., and Koningsberger, D. C., *Catal. Lett.* **62**, 15 (1999).
18. van den Broek, A. C. M., van Grondelle, J., and van Santen, R. A., *J. Catal.* **167**, 417 (1997).

19. de Graaf, J., van Dillen, A. J., de Jong, K. P., and Koningsberger, D. C., *J. Catal.* **203**, 307 (2001).
20. Kinoshita, K., Routsis, K., and Bett, J. A. S., *Thermochim. Acta* **10**, 109 (1974).
21. Dalla Betta, R. A., and Boudart, M., *in* "Proceedings, 5th International Congress on Catalysis, Palm Beach, 1972" (J. W. Hightower, Ed.), p. 1329. North Holland, Amsterdam (1973).
22. Keegan, M. B. T., Dent, A. J., Blake, A. B., Conyers, L., Moyes, R. B., Wells, P. B., and Whan, D. A., *Catal. Today* **9**, 183 (1991).
23. Zou, W., and Gonzalez, R. D., *J. Catal*. **133**, 202 (1992).
24. Muñoz-Páez, A., and Koningsberger, D. C., *J. Phys. Chem.* **99**, 4193 (1995).
25. Koningsberger, D. C., and Prins, R., "X-Ray Absorption. Principles, Applications, Techniques of EXAFS, SEXAFS and XANES." Wiley, New York, 1988.
26. Scholten, J. J. F., Pijpers, A. P., and Hustings, A. M. L., *Catal. Rev.–Sci. Eng.* **27**, 151 (1985).
27. Vaarkamp, M., Mojet, B. L., Modica, F. S., Miller, J. T., and Koningsberger, D. C., *J. Phys. Chem.* **99**, 16067 (1995).
28. Ramaker, D. E., Mojet, B. L., Koningsberger, D. C., and O'Grady, W. E., *J. Phys. Condens. Matter* **10**, 8753 (1998).
29. Koningsberger, D. C., Mojet, B. L., van Dorssen, G. E., and Ramaker, D. E., *Top. Catal.* **10**, 143 (2000).
30. van Dorssen, G. E., Ramaker, D. E., and Koningsberger, D. C., submitted for publication.
31. Zabinsky, S. I., Rehr, J. J., Ankudinov, A., Albers, R. C., and Eller, M. J., *Phys. Rev. B* **52**, 2995 (1995).
32. Koningsberger, D. C., *in* "Hercules Course. Neutron and Synchrotron Radiation for Condensed Matter Studies. Applications to Solid State Physics and Chemistry" (J. Baruchel, J. L. Hodeau, M. S. Lehmann, J. R. Regnard, and C. Schlenker, Eds.), Vol. 2, Chap. X. p. 213. Springer-Verlag, Berlin/New York, 1994.
33. Oudenhuijzen, M. K., Bitter, J. H., and Koningsberger, D. C., *J. Phys. Chem. B* **105**, 4616 (2001).
34. Kip, B. J., Duivenvoorden, F. B. M., Koningsberger, D. C., and Prins, R., *J. Catal.* **105**, 26 (1987).
35. Homeyer, S. T., and Sachtler, W. M. H., *J. Catal.* **117**, 91 (1989).
36. Homeyer, S. T., and Sachtler, W. M. H., *in* "Zeolites" (P. A. Jacobs and R. A. van Santen, Eds.), p. 984. Elsevier, Amsterdam, Netherlands, 1989.
37. Majumdar, D., Dai, D., and Balasubramanian, K., *J. Chem. Phys.* **113**, 7928 (2000).
38. Homeyer, S. T., and Sachtler, W. M. H., *J. Catal.* **118**, 266 (1989).
39. Borgna, A., Garetto, T. F., Apesteguía, C. R., LeNormand, F., and Moraweck, B., *J. Catal.* **186**, 433 (1999).